Fuel Processing Technology 263 (2024) 108129

Contents lists available at ScienceDirect

Fuel Processing Technology

journal homepage: www.elsevier.com/locate/fuproc

A simultaneous depolymerization and hydrodeoxygenation process to produce lignin-based jet fuel in continuous flow reactor

Adarsh Kumar [a,b], David C. Bell [a], Zhibin Yang [a], Joshua Heyne [a], Daniel M. Santosa [c], Huamin Wang [c], Peng Zuo [d], Chongmin Wang [d], Ashutosh Mittal [b], Darryl P. Klein [e], Michael J. Manto [e], Xiaowen Chen [f], Bin Yang [a,d,*]

[a] Bioproducts, Sciences, and Engineering Laboratory, Department of Biological Systems Engineering, Washington State University, Richland, Washington 99354, United States
[b] Renewable Resources and Enabling Sciences Center, National Renewable Energy Laboratory, Golden, CO 80401, United States
[c] Energy Processes & Materials Division, Pacific Northwest National Laboratory, Richland, Washington 99352, United States
[d] Environmental Molecular Sciences Laboratory, Pacific Northwest National Laboratory, Richland, Washington 99354, United States
[e] Advanced Refining Technologies, LLC, Baltimore, MD, United States
[f] National Bioenergy Center, National Renewable Energy Laboratory, Golden, CO 80401, United States

ARTICLE INFO

Keywords:
Continuous flow reactor
Engineered catalyst
Lignin-based jet fuel
Simultaneous depolymerization and hydrodeoxygenation
Tier α fuel property

ABSTRACT

Economical production of lignin-based jet fuel (LJF) can improve the sustainability of sustainable aviation fuels (SAFs) as well as can reduce the overall greenhouse gas emissions. However, the challenge lies in converting technical lignin polymer from biorefinery directly to jet fuel in a continuous operation. In this work, we demonstrate a simultaneous depolymerization and hydrodeoxygenation (SDHDO) process to produce lignin-based jet fuel from the alkali corn stover lignin (ACSL) using engineered Ru-HY-60-MI catalyst in a continuous flow reactor, for the first time. The maximum carbon yield of LJF of 17.9 wt% was obtained, and it comprised of 60.2 wt% monocycloalkanes, and 21.6 wt% polycycloalkanes. Catalyst characterization of Ru-HY-60-MI suggested there was no significant change in HY zeolite structure and its crystallinity after catalyst engineering. Catalyst characterizations performed post the SDHDO experiments indicate presence of carbon and K content in the catalyst. K content presence in the spent catalyst was due to K^+ ion was exchanged between lignin solution and HY-60 while carbon presence validated the SDHDO chemistry on the catalyst surface. Tier α fuel property testing indicates that LJF production using SDHDO chemistry can produce SAF with high compatibility, good sealing properties, low emissions, and high energy density for aircraft.

1. Introduction

Global jet fuel consumption was 95 billion gallons in 2019 [1]. Jet fuel consumption has been hampered significantly in the last three years because of restricted air travel during the COVID-19 pandemic, however, demand is expected to be 32 % higher in 2030 and more than double by 2050 of 2019 levels [2]. Meanwhile, environmental pollution is and will be a growing concern in the aviation industry. SAFs emerge as potential solutions that can reduce contrail formation and carbon footprints and help meet the net carbon neutrality policy of the United Nations [3,4]. Most market-available SAFs are synthesized using plant- and animal-derived lipid feedstocks (ASTM D7566 Annex 2) [5–9]. The limited availability of these feedstocks does not produce SAFs in the volumes required to meet the expected future demand. It is commonly agreed that a multitude of new pathways will be necessary to meet the 2050 goal.

One limitation of many SAFs is their inability to provide swelling of fuel system seals, high density, and other components (ASTM D1655). Many airlines limit the direct use of these SAF and balance their fuel with conventional jet fuel (CJF) to rectify these concerns [10,11]. These limitations are primarily due to the lack of aromatics and cycloalkanes in these SAFs [12,13]. Aromatics and cycloalkanes are two of the primary hydrocarbon classes in CJF, composing on average 20 % and 21 % of the total hydrocarbons [14], respectively. Fuel testing properties suggest

* Corresponding author at: Bioproducts, Sciences, and Engineering Laboratory, Department of Biological Systems Engineering, Washington State University, Richland, Washington 99354, United States
E-mail address: bin.yang@wsu.edu (B. Yang).

https://doi.org/10.1016/j.fuproc.2024.108129
Received 7 May 2024; Received in revised form 12 July 2024; Accepted 25 August 2024
Available online 2 September 2024

their presence in CJF is valuable. However, aromatics are known to be the primary culprit for soot formation, which has numerous negative environmental and human health consequences, causing some interest in trying to remove them from the fuel entirely. A fuel needs aromatics to meet density and material compatibility requirements. Cycloalkanes have been identified as a potential low sooting substitute for aromatics providing comparable density as well as some seal swell at a higher concentration [15,16]. This opens the conversation about whether they can be used to replace aromatics entirely to reduce sooting potential.

Lignin has the capacity to produce a largely produced (300 million tonnes/year) aromatic structure-based polymer [17]. These aromatic structures can act as the base to produce fuels, chemicals, and materials [18–21]. Several studies from our groups at Washington State University, USA showed the direct catalytic depolymerization and hydrodeoxygenation of lignin into C7–C18 jet fuel range hydrocarbons having mainly cycloalkane (1/3–2/3 wt%), including alkyl-substituted mono-, bi-, and tri-cyclohexyl alkanes (US patent 9,518,076 B2 and US patent 11,078,432 B2) [22–35].The catalytic process involves catalytic depolymerization and hydrodeoxygenation of lignin using Ru-based bifunctional catalysts, Ru/C + $ZnCl_2$, Ru/Al_2O_3, Ru/HY, Ru-M/HY (M = Fe, Ni, Cu, Zn) and Ru/HY + triflate. Among them, Ru/HY was the most active and selective. A recent blending effect study demonstrated that 10 vol% blending of this LJF with CJF have an equivalent surface tension, density, viscosity, derived cetane number, and flash point to CJF [10,32]. The success from this study warrants further research into continuous processes, which are more viable for commercialization. Commercial scale production will help to realize the environmental benefits of sustainable aviation fuel [36,37]. Previous studies on LJF utilized a batch process, and a techno-economic assessment suggests that jet fuel blend stocks can be produced using technical lignin and HDO technologies at costs that approach commercial feasibility. To achieve the commercial production goal of LJF, a continuous process is required. Several recent reports are available on the continuous flow catalytic reactors [38–40]. However, they used the lignin in form of oil after multistep processing at high temperatures. This work distinguishes itself by using solid technical lignin instead of extracted lignin oil form. Furthermore, this study primarily produces cycloalkanes, whereas these reported findings focus on producing a mixture of aromatics.

Addressing the challenges posed by the heterogeneous nature of lignin is crucial for successful technical lignin processing in continuous flow reactors. In this study, we present a novel SDHDO of technical lignin to generate LJF, focusing on preventing rapid reactor blockage. We overcame the complexities of direct lignin conversion and the preservation of cyclic structures in the product by employing innovative reaction engineering techniques. Through comprehensive product analysis using GC–MS and GCxGC-FID, we confirmed the successful production of a mixture of cycloalkanes enriched with alkylated side-chains spanning from C_7 to C_{18}. Overall, LJF can open the door to new types of SAF blends having equivalent or better o-ring sealing properties, very low emissions, and high energy density while remaining ‘drop-in’.

2. Materials and methods

2.1. Materials

$RuCl_3$.hydrate purchased from Johnson Matthey. HY Zeolite (CBV400) bought from Zeolyst international. Ethyl acetate, K_2CO_3, H_2SO_4, and NaOH procured from Fisher-Scientific. Milli Q water was prepared in the lab. DMR black liquor of ACSL was supplied from National Renewable Energy Laboratory (NREL).

2.2. Catalyst synthesis

The design and synthesis of efficient and engineered bifunctional catalyst for the direct lignin HDO is challenging. Because competition between depolymerization, ring saturation and C − O hydrogenolysis create difficulty to originate ring saturated hydrocarbons. Acidic support is active for depolymerization, while a highly dispersed active metal is required for H_2 activation. An excellent combination of these properties can be an effective catalyst for saturated hydrocarbon production. With the same aim, 60 % HY zeolite extrudates was synthesized by using 40 % inert material (pseudoboehmite alumina powder) and 60 % HY Zeolite powder. Extrudates used for impregnation of an aqueous $RuCl_3$ solution containing 0.104 g $RuCl_3$ with 0.10 g citric acid per mL water. Ru loading was controlled to 2 wt%, and an extra amount of water was used to fill the pores of HY extrudates. The resultant catalyst was named Ru-HY-60-MI. The prepared catalyst was dried and subsequently calcined at 500°C under continuous air flow for 0.5 h. Calcined catalyst was washed multiple times with hot water to remove the remaining citric acid. Washed catalyst was again dried and sieved using mesh size (60–80) before using in the experiment. The detailed procedure in pictorial form is given in the Fig. S1.

2.3. Characterization methodologies

Surface area, pore size and pore volume of catalysts were assessed using N_2-porosometry. Inductively coupled plasma atomic emission spectroscopy (ICP-AES) used to see the compositions of fresh and spent Ru-HY-60-MI. Carbon monoxide pulse chemisorption and H_2-temperature programmed reduction (H_2-TPR) of Ru-HY-60-MI were carried out for metal dispersion and reduction profile of catalyst. The acidity of Ru-HY-60-MI was determined using temperature-programmed desorption (TPD) using NH_3 as a probe molecule. Scanning transmission electron microscopy (STEM) studies were performed for imaging and textural assessment. X-ray diffraction (XRD) of catalysts were recorded for the determination of crystallinity and structure of catalysts. The details of each methodology are given in supplementary.

2.4. Reaction procedure

5 g purified lignin was dissolved in 1 wt% aqueous solution of K_2CO_3. A trickle bed reactor setup (Fig. 1) having metal to metal contact reactor (hastelloy C276) and dual stage furnace was used for SDHDO. 10 g Ru-HY-60-MI (60–80 mesh size) was packed in reactor with 0.75-in.

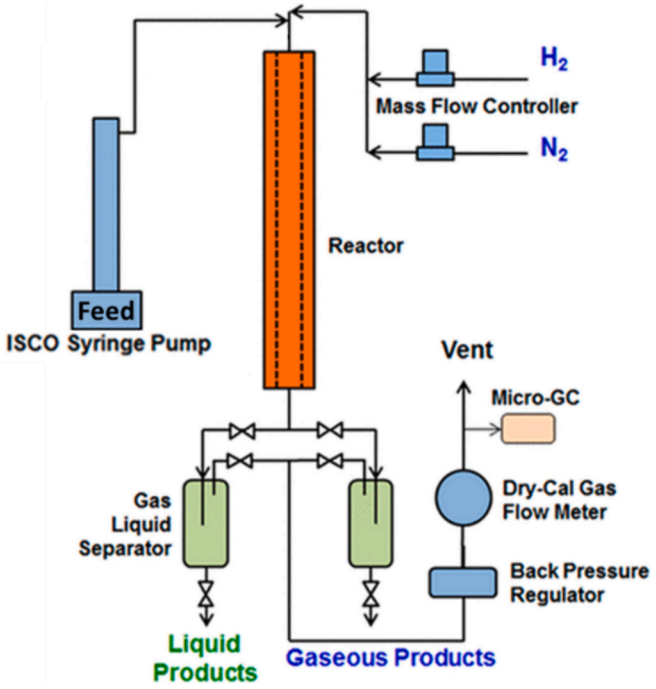

Fig. 1. Trickle bed reactor used for direct and continuous SDHDO of lignin.

diameter and length of 26 in.. The catalyst bed length was 4 in., and the volume of catalyst was 14 mL. Catalyst was reduced *in situ* at reaction temperature with 300 mL min^{-1} flow of pure hydrogen before experiment. The mass flow controller and back-pressure regulator were controlling the gas flow and pressure in the reactor. High-pressure feeding pump was used to supply lignin solution after reaching the reaction conditions. The gas product of experiment analysed in online 4-channel gas chromatography (Inficon 3000) and volume of gas calculated using the out-flow gas data of flowmeter (Drycal®). Temperature and pressure were monitored by Labview® software with both temperature and pressure sensors of the reactor system within ±2 % error. The liquid product collected in gas-liquid separator and this vessel drained at regular interval to store the sample for further analysis. Each experiment was performed on the fresh catalyst bed.

2.5. Product analysis

The organic phase from total liquid was extracted with ethyl acetate. The ethyl acetate extracted organic phase examined in GCXGC-FID and GC -MS for quantitative and qualitative identifications.

1 μL sample in the splitless mode was injected to DB-5 capillary column (30 m × 250 μm × 0.25 μm) in GC (Agilent Technologies 7890A)-MS (Agilent Technologies 5975C) with 0.6 mL min^{-1} flow of helium for qualitative analysis. The GC oven was programmed; 40 $^{\circ}C$ for 3 min, then temperature raised to 200 $^{\circ}C$ at 15 $^{\circ}C$ min^{-1} (3 min hold time), subsequently temperature ramped to 280 $^{\circ}C$ at 5 $^{\circ}C$ min^{-1} and was held at this temperature for 5 min. Eluting compounds were identified using NIST library (2008).

Hydrocarbon type analysis was performed using two-dimensional gas chromatography (GC × GC) with flame ionization detector (FID). An Agilent 8890 gas chromatograph with a split/splitless injector (Agilent Technologies, Inc., CA, USA), and a Sepsolve INSIGHT flow modulator. This experiment is also equipped with a VGA-101 (VUV Analytics, TX, USA), however this data is not used in this study. The GC is equipped with a polar 1st column (Rxi-17Sil MS, 60 m × 0.32 mm × 0.5 μm) and a non-polar 2nd column (Rxi-1 ms, 15 m × 0.32 mm × 0.5 μm). Chromatographic integration was performed using ChromSpace software. Hydrocarbon group quantification was performed following the method described by Johnson et al. [41].

2.6. Calculations

The calculations of solid, liquid and gases were based on carbon content in products vs technical lignin. The yield of compounds was dependent on the weight of compounds [42]. All results are reported with ±3 % error.

$$\text{Carbon content in solid, \%} = \frac{\text{Carbon content in spent catalyst} - \text{Carbon content in fresh catalyst}}{\textit{Carbon content in lignin}} \times 100$$

$$\text{Carbon content in gas, \%} = \frac{\textit{Carbon content in gas (based on GC} - \textit{TCD)}}{\textit{Carbon content in lignin}} \times 100$$

$$\text{Carbon content in liquid, \%} = (\%, \text{Carbon content in ACSL} - (\%, \text{Carbon content in gas} + \text{Carbon content in solid})$$

$$\text{Yield of product A, \%} = \frac{\text{Weight of product A}}{\textit{Weight of total liquid products}} \times 100$$

3. Results and discussion

3.1. Simultaneous depolymerization and HDO of lignin

SDHDO of ACSL was investigated to produce LJF. NREL used dilute alkali (0.1 mol L^{-1} NaOH) deacetylation and mechanical refining treatment to separate lignin from corn stover [43]. Lignin obtained from NREL had a big portion (ca. 80 %) of insoluble lignin solid at pH 3. Lignin amount and carbon content were calculated (Supplementary, Tables S1 and S2) after purification (Supplementary, Fig. S2) [28]. Monolignols groups in the native lignin are interconnected by etheric C—O linkages (β–O–4′, 4–O–5′) and C—C linkages (β–β', β–1′, β–5′, and 5–5′). A several modifications occurred in β–5′, 5–5′ and β–O–4′ linkages during lignin separation process which reflects in lignin structure [33,44,45]. Two-dimensional heteronuclear single quantum coherence NMR estimated amounts of β-O-4′, β-5′, β–β', and β-1′ inter-unit linkages in the purified biorefinery lignin [28]. Normalized amounts of these were 43, 44, 9, and 4 %, respectively [28]. Carbon distribution in solid, gas and liquid (Fig. 2a), along with product distribution in liquid (Fig. 2b), both, revealed critical importance of selecting reaction parameters in the SDHDO. Hence, we systematically changed temperature, pressure, and feed flow to evaluate the impact of these on SDHDO.

Low temperature achieved high carbon content in the liquid by preserving methoxy groups on aromatic ring (Fig. 2b) at 1150 PSI hydrogen pressure and 20 mL min^{-1} feed flow. It suggests that 225 $^{\circ}C$ is effective for C-O-C bond cleavage in lignin depolymerization [46]. A high number for aromatic hydrocarbons compared to aliphatic indicates fast deoxygenation ability of catalyst than hydrogenation because of low metal content and low temperature [47–50]. High temperature favoured the complete hydrodeoxygenation of depolymerized lignin products, and a clean hydrocarbon liquid obtained at 250 $^{\circ}C$ with 17.9 % carbon yield. These results are in well aligned with our previous reports in batch reactors at same temperature [23,25,51,52]. GC–MS (Fig. 2) and GCxGC-FID analysis (next section) confirmed the presence of complete in-depth hydrodeoxygenated compounds in the product. Moreover, the clear and transparent droplets of hydrocarbons can be seen on water surface (Fig. S3). Product distribution in the liquid suggested the major number of monocyclic aliphatic hydrocarbons with some monocyclic aromatic hydrocarbons. However, a significant amount of C_{12+} polycyclic aliphatic hydrocarbons identified. This implied two hypothesis, i) the HDO of released dimers with C—C linkages from ACSL and well supported with the structural characteristics of ACSL [28,33], ii) formation of dimers over acidic catalysts due to the well-known mechanism of electrophilic aromatic substitution via cyclohexyl cation pathway [53,54]. Further increase in temperature drastically changed the product profile and a huge drop in liquid carbon yield can be seen in Fig. 2a. A notable increase in solid (52.8 %) and strong rise in the carbon yield of gas (14.5 %) suggest that gasification was the primary reaction at 275 $^{\circ}C$ instead of SDHDO [55,56]. Similarly, disappearance of polycyclic aliphatic hydrocarbons and low presence of monocyclic aliphatic hydrocarbons with a bulk existence of light C_5 and C_6 hydrocarbons at 275 $^{\circ}C$ indicates temperature sensitive cracking of cyclic aliphatic hydrocarbons [53,57].

Next, hydrogen pressure effect was examined at 250 $^{\circ}C$ and 20 mL

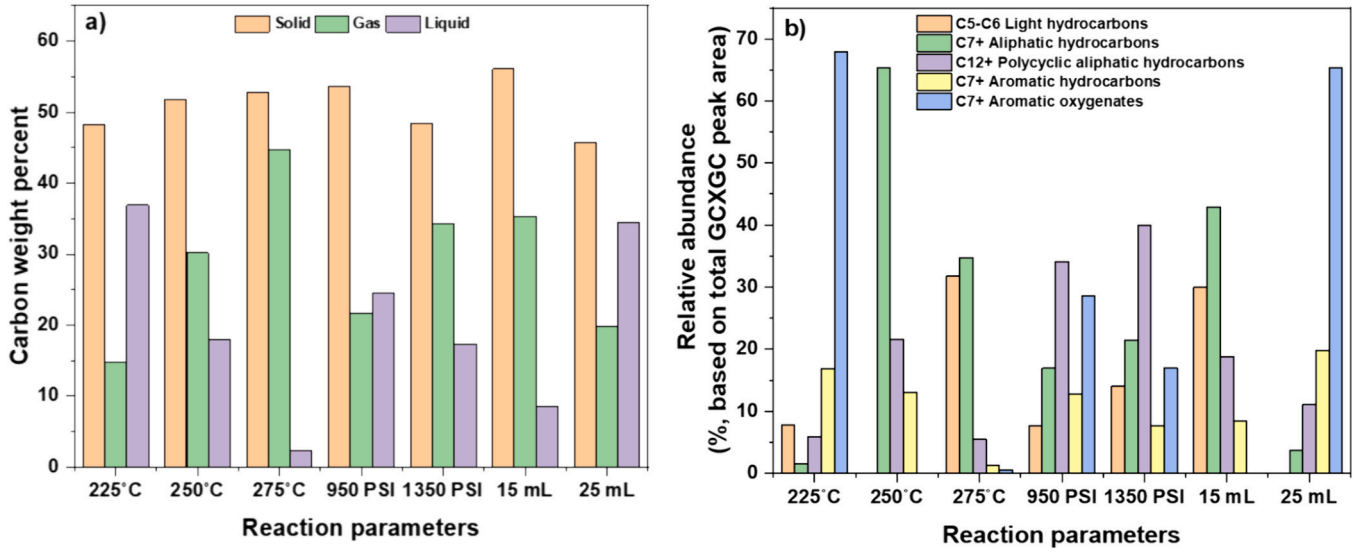

Fig. 2. Lignin conversion over engineered Ru-HY-60-MI; a) carbon distribution in gas, liquid and solid; b) type of products identified in liquid. Rection conditions: Ru-HY-60-MI- 10 g, Feed – 5 wt% lignin in 1 wt% K_2CO_3 aqueous solution, Feed flow – 20 mL h^{-1}, T – 250°C, Pressure – 1150 PSI, Hydrogen flow – 300 mL min^{-1}. 15 mL and 25 mL in figures show feed flow per hour. The changed conditions are mentioned in graph when changed during the experiment.

min^{-1} feed flow. The depletion carbon content of solid and scaled carbon in gas with pressure showed a positive impact of pressure on ACSL depolymerization. Whereas the overall recovery carbon in liquid is highest for 950 PSI (Fig. 2a) and validated with ~28.6 % aromatic oxygenates having different functional groups. However, low availability of jet fuel range hydrocarbons in the liquid product suggests partial deoxygenation of ACSL at 950 PSI. 1150 PSI results in complete hydrodeoxygenation of formed aromatics oxygenates and yield jet fuel range hydrocarbons. This phenomenon implies that 1150 PSI tunes the product profile owing to high availability of hydrogen on catalyst surface and resulted efficient SDHDO [58]. Further increase in pressure resulted in high monomers, high dimers and again the appearance of aromatic oxygenates with minimum solid and maximum gas. This suggests, pressure enhanced the cracking of formed products and concurrent depolymerization of ACSL [59]. However, these phenomena might be deactivating the catalytic active sites which subsequently showed resistant towards HDO reactions [60]. Improved dimers yield with pressure validates electrophilic aromatic substitution pathway hypothesis of dimers formation [61]. The carbon content trend was reverse of solid, liquid and gas with feed flow change compared to temperature and pressure change. The light hydrocarbons appeared at 15 mL min^{-1} feed flow and these disappeared with an increase in flow. This occurred due to low availability of reacting molecules vs. active sites at 15 mL min^{-1} feed flow and lead to in hydrocracking of ACSL [62]. The presence of huge aromatic oxygenates with aromatic hydrocarbons at 25 mL min^{-1} feed flow suggests that the available active sites are insufficient for complete HDO. This phenomenon is reflected in high carbon yield within liquid.

These above results and discussion suggest that all reaction parameters significantly affect the lignin conversion and product profiles. An adequate amount of carbon in solid at all reaction conditions indicates the presence of unbreakable C—C bonds in lignin. This reveals the bond dissociation enthalpies of C—C linkages are 100 and 200 kJ mol^{-1} higher than C–O–C linkages: α–O–4′ (215 kJ mol^{-1}) < β–O–4′ (290–305 kJ mol^{-1}) < β–1′ (360–390 kJ mol^{-1}) < 5–5′ (490 kJ mol^{-1}) [63–65].

Identification of a nonreactive suitable solvent to dissolve lignin for continuous feeding in reactor is another level of difficulty. With this aim, ACSL was solubilized in sodium hydroxide. Initially, a mass fraction of 5 % ACSL in 1 wt% aqueous sodium hydroxide was tested, but the catalyst was deactivated very quickly. A complete gasification was observed with 1 % lignin. We were able to see the hydrocarbon product with 5 % ACSL in 0.5 wt% NaOH aqueous solution. However, the catalyst was still deactivating fast. The relative abundance of hydrocarbons was very poor compared to K_2CO_3 dissolved ACSL (Fig. 3). Practically, when NaOH was used as ACSL dissolution solvent there was high ion exchange with HY-60 zeolite due to smaller Na^+ ion (Table 1), simultaneously the pH of feed was quite high (12.4 vs 8.6 with K_2CO_3) [66]. These factors were responsible for rapid deactivation of the catalyst.

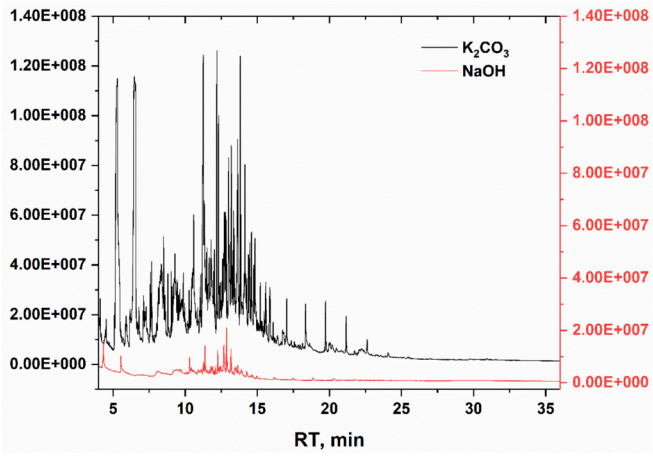

Fig. 3. Impact of ACSL solubilizing agent K_2CO_3 Vs NaOH. Reaction conditions: Feed – 5 wt% Lignin in K_2CO_3 (1 wt%)/NaOH (0.5 wt%), Ru-HY-60-MI: 10 g, Temp – 250°C, P- 1150 PSI, Feed flow – 20 mL h^{-1}, Hydrogen flow – 300 mL min^{-1}. Same amount of feed supplied, and same amount of extractive solvent used.

3.2. *Tier α characterization of Lignin-derived cycloalkanes jet fuel*

The detailed hydrocarbon type analysis on LJF performed on GCxGC-FID is shown in Fig. 4 and Fig. S4. LJF contains 81.8 wt% cycloalkanes, 5.2 % n-alkanes and isoalkanes and 13.1 % aromatics. Within cycloalkanes, 60.2 % were monocycloalkanes, and 21.6 % were polycycloalkanes. Within the aromatics fraction, 5.7 % was alkyl derivates of benzene, 3.9 % were diaromatics and 3.5 % belonged to the cycloalkanes-aromatics group. Average carbon number of LJF is 10.9 (Fig. 3), which is very close to the carbon average number of

Table 1
Physio-chemical characteristics of the catalyst samples.

Catalyst	Ru, wt%	Na, wt%	K, wt%	Surface area, $m^2\ g^{-1}$	Pore volume, $cm^3\ g^{-1}$	Average pore diameter, nm
HY-60-Extrudate	–	0.85	0.03	468	0.46	0.86
Ru-HY-60-MI	2.07	0.63	0.02	467	0.43	0.82
S-Ru-HY-60-MI	2.77	0.65	1.87	141	0.17	0.64
S-NTT-Ru-HY-60-MI	1.76	0.59	1.95	43	0.07	0.75
S-Ru-HY-60-MI-Na	2.17	3.15	0.04	138	0.19	0.64

Ru, Na, K: Inductively coupled plasma atomic emission spectroscopy (ICP-AES).
Physicochemical characteristics: Nitrogen porosity.
S: Spent catalyst with thermally treatment at 550 °C.
S-NTT: Spent catalyst not thermally treated.
S-Ru-HY-60-MI-Na: 0.5 wt% aqueous NaOH solution was used to dissolve lignin for experiment.

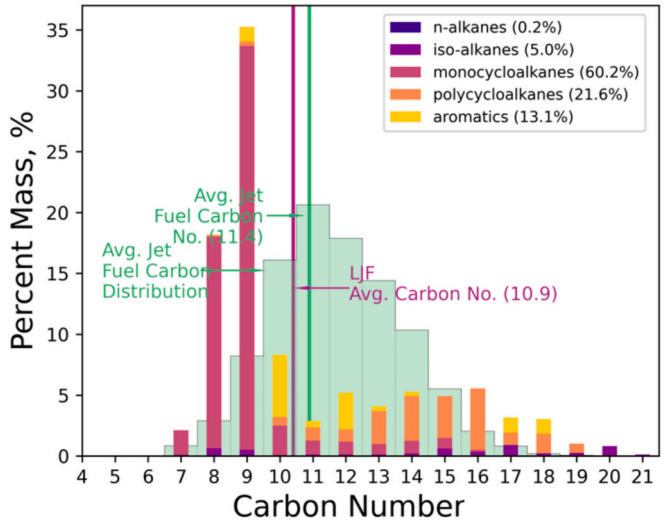

Fig. 4. Hydrocarbon type analysis on LJF, different hydrocarbon group is represented using various colors and the same carbon number group are stacked on top of each other. The average conventional jet fuel carbon distribution (green shaded region) and average carbon number. (For interpretation of the references to colour in this figure legend, the reader is referred to the web version of this article.)

conventional jet fuel (11.4) [67,68].

To validate the compatibility of LJF in the existing commercial aircrafts the tier α properties of LJF were tested. However, due to the limited volume of the LJF sample, physical property measurements were not feasible, prediction was performed instead [67]. The tier α property prediction was performed based on the detailed hydrocarbon composition of the LJF. Predicted properties including surface tension (σ), density (ρ), kinematic viscosity (ν), lower heating value (LHV), flash point, derived cetane number (DCN), and freeze point for LJF are shown in Fig. 4. Both full distillate LJF (blue triangle), virtual distilled LJF (black circle) and 68 and 95 percentile confidence intervals (solid line and dash line) were reported as well, more detailed on the prediction method could be found here [67]. LJF showed a comparable surface tension, density, viscosity, LHV, and freeze point as to CJF. The flash point violation in the full distillate LJF is caused by an elevated concentration of light hydrocarbons ($<C_8$) (Fig. 5). This flash point violation could be resolved by removing the front 21 % of the sample (all C_7 and C_8) by distillation as the black circle shown on Fig. 4. DCN of this sample is expected to be lower than average CJF, since cycloalkanes makeup 81.8 % of the sample, they are known to have a lower DCN compared to n and isoalkanes due to the ring structure [69]. DCN of CJF is increased by having n and isoalkanes in the mixture. The high concentration of cycloalkanes in LJF offers a complementary synergy blending with current existing pathway that produce mostly (n and isoalkanes). Where

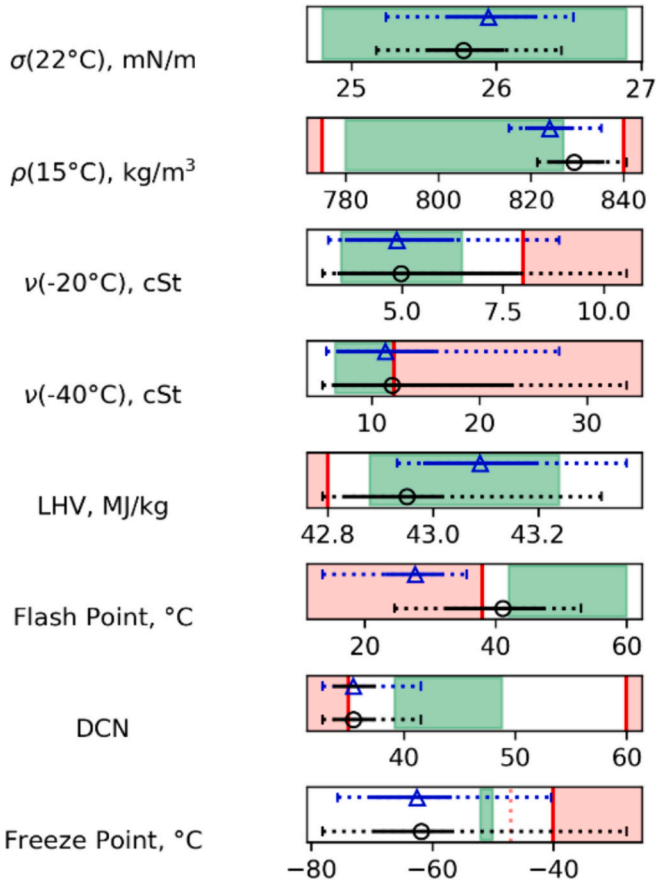

Fig. 5. Tier α predictions on full distillate LJF (blue triangle and lines) and virtual distilled LJF (black circle and lines), the conventional fuel experience range (green shaded region), ASTM D7566 specification limit (red bar), and violation of specification (red shaded region) is shown for reference. (For interpretation of the references to colour in this figure legend, the reader is referred to the web version of this article.)

LJF offers the required density and seal swell that n and isoalkanes could not achieve, and n and isoalkanes would boost the DCN of the blended fuel into the specification limit.

3.3. Characteristics of catalysts

3.3.1. Ru-HY-60-MI characterization

Pore diameters and pore volume data show that these values are higher for engineered extrudates than the parent HY (Table 1). BET surface area is almost the same for Ru-HY-60-MI and engineered extrudates. It might be due to the high dispersion and small Ru

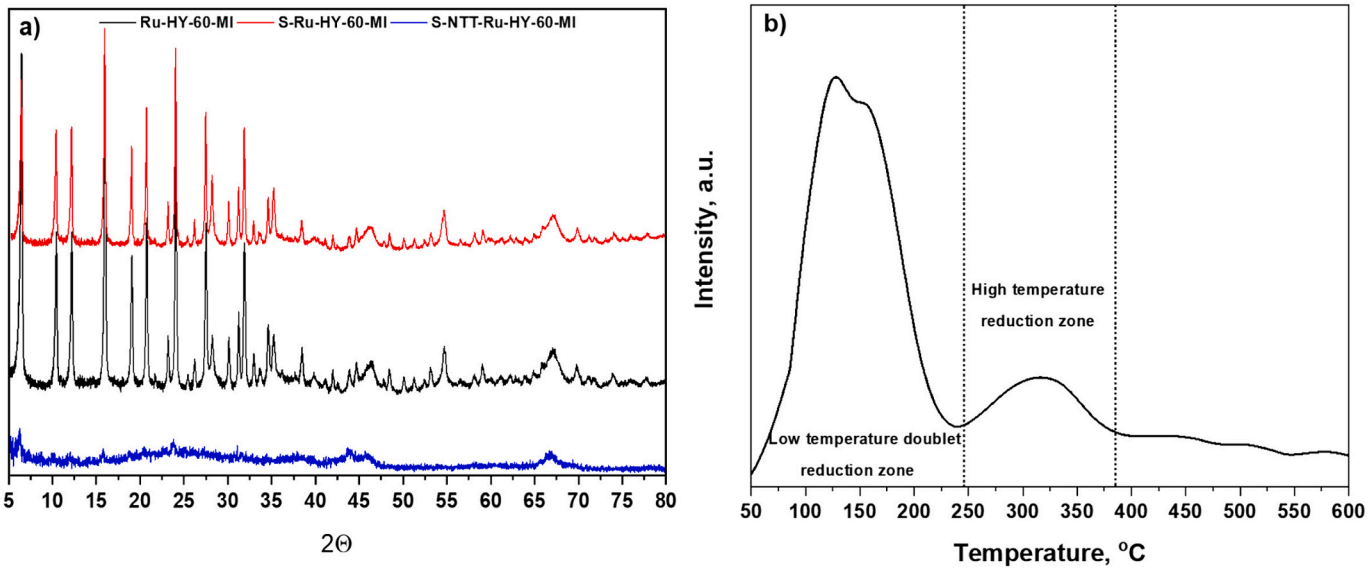

Fig. 6. a) XRD patterns of Ru-HY-60-MI, S-Ru-HY-60-MI, S-NTT-Ru-HY-60-MI; b) TPR profile of Ru-HY-60-MI.

nanoparticles. The decrease in pore size of Ru-HY-60-MI (0.04 nm) is caused by the presence of small ruthenium nanoparticles within the pores, which is supported by low pore volume data [32]. ICP analysis of Ru-HY-60-MI indicates actual Ru loading (2.07 wt%) is close to theoretical value (2.0 wt%) and legitimate the catalyst synthesis methodology. However, there were tiny impurities, such as Na and K present with Ru, Si, Al, O.

XRD of Ru-HY-60-MI reflects identical crystalline pattern to HY zeolites at 6.1, 10.3, 15.9 and 23.9° (Fig. 6a). The observation suggesting there was no significant change in HY zeolite structure and its crystallinity after catalyst engineering [51]. Non-appearance of Ru peak after metal impregnation indicating Ru particle size is significant low with high dispersion. Chemisorption analysis assisted high Ru dispersion fact, which was 16.2 %. TPR profile of the Ru-HY-60-MI exhibits two reduction zones $\leq 250^{\circ}C$ and $\geq 250^{\circ}C$ (Fig. 6b), indicating two different types of reduction of RuO_X. The narrow peak ($\geq 250^{\circ}C$) is corresponding to the reduction of RuO_3 in RuO_2 [70]. Moreover, an intense TPR peak ($\leq 250^{\circ}C$) of Ru-HY-60-MI starts at lower temperature in a doublet form

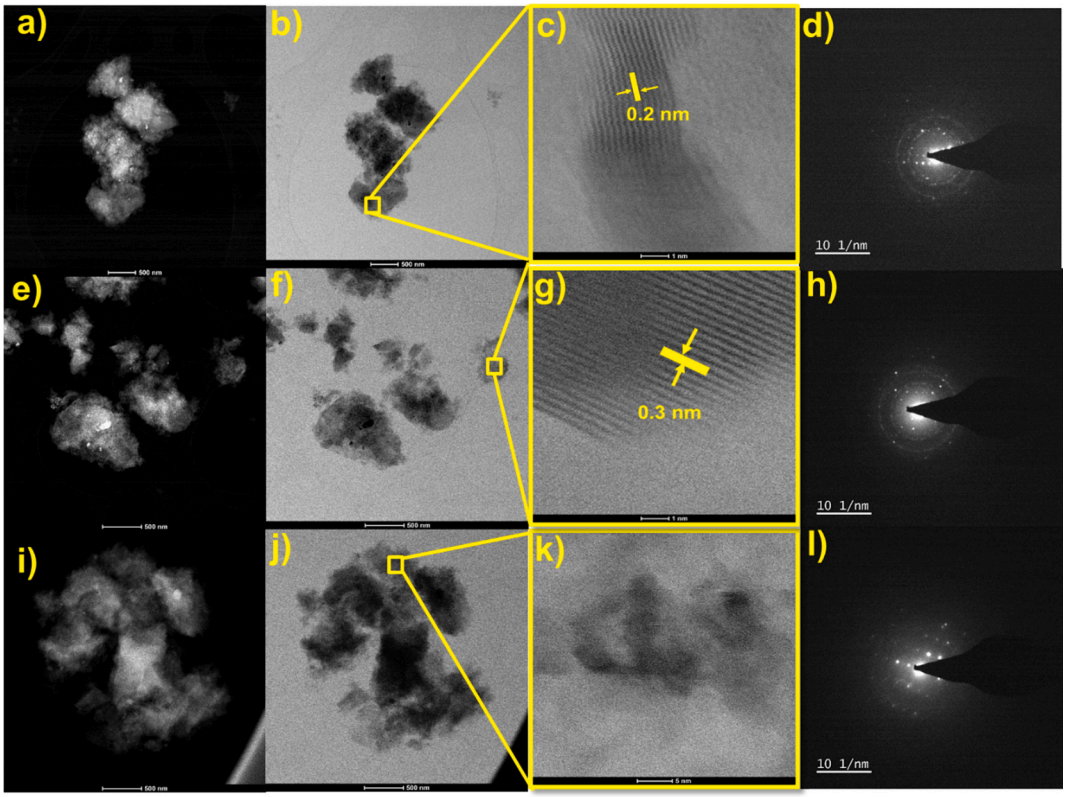

Fig. 7. Structural and chemical analysis of Ru-HY-60-MI (the top row), S-Ru-HY-60-MI (the mid row) and S-NTT-Ru-HY-60-MI (the bottom row) by TEM. (a,e,i) STEM- high-angle annular dark field (STEM-HAADF) and (b,f,j) STEM- bright field (STEM-BF) images of prepared catalysts; (c,g,k) STEM-BF images along with measured interplanar spacing; (d,h,l) Ru STEM-EDS mapping [53].

suggesting the different location of a high number of smaller RuO_2 species on/in the zeolite structure [71,72].

XRD and TPR results can be supported well by the STEM observation to validate small Ru size and its good dispersion over HY-60 support [73]. STEM analysis of Ru-HY-60-MI shows most of Ru particles diameter was ≤5 nm with average size of 2.9 ± 0.05 nm. It means Ru was below the detection limit of XRD [74]. The elemental analysis identified Ru, O, Al, Si in catalysts (Fig. S5) and STEM-EDS exhibits almost homogeneous distribution of Ru in Ru-HY-60-MI (Fig. 7). Selected-area electron diffraction (SAED) pattern indicates highly crystalline HY zeolite structure and further abetted XRD results that despite the modification of zeolite composition, there was no change in zeolite structure. Captured lattice fringes from Ru in Ru-HY-60-MI suggests that both cubic and hexagonal Ru are possible to be formed in Ru-HY-60-MI (measured: 0.2 nm; cubic: d111 = 2.19 Å, d200 = 1.90 Å; hexagonal: d002 = 2.14 Å, d1–11 = 2.06 Å) [75,76]. NH_3-TPD profile of Ru-HY-60-MI attributes two types of acidities. Weak acidic sites are found between 100 and 200 $^{\circ}C$ and strong acid sites are in a range of 300–500 °C, which is similar to HY zeolite [77] (Fig. S6).

3.3.2. *Spent Ru-HY-60-MI characterization*

ICP analysis of S-Ru-HY-60-MI indicates a significant increase in K content. Moreover, drastic changes in surface area, pore volume and pore size had appeared after the experiment (Table 1, entry 4). This resulted in carbon being deposited on the Ru-HY-60-MI surface and the exchange of K^+ ions from lignin solution to HY-60. These factors were responsible for catalyst deactivation [78,79]. Elemental compositions of S-NTT-Ru-HY-60-MI using STEM-EDS validates the presence of carbon and K content in spent catalyst (Supplementary, Table S3). The lattice fringes cannot be seen in high resolution STEM image of S-NTT-Ru-HY-60-MI because of surface coverage (Fig. 6l). Moreover, the ring pattern in the SAED image was absent, indicates S-NTT-Ru-HY-60-MI is low in crystalline nature. Similarly, all peaks of HY zeolite have disappeared in the XRD of S-NTT-Ru-HY-60-MI due to carbon coverage on the catalyst surface. However, the crystallinity can be further seen after thermal treatment of this at 550 $^{\circ}C$ under air environment (S-Ru-HY-60-MI). Likewise, clean STEM images captured for the S-Ru-HY-60-MI (Figs. 6e-6h) indicating the surface of S-Ru-HY-60-MI has been cleansed in thermal treatment [79]. These all factors support each other's and validate the hypothesis.

4. Conclusions

Challenges associated with complex reaction engineering during the direct conversion of lignin, with the goal of producing LJF, were addressed in the context of continuous flow lignin conversion. Engineered Ru-HY-60-MI successfully demonstrated a continuous lignin to LJF process via SDHDO for the first time. The carbon yield of LJF was 17.9 wt% at optimum reaction conditions. The qualitative and quantitative product analysis using GC–MS and GCxGC-FID confirmed the production of cycloalkanes mixture rich with alkylated sidechains ranging between C_7 and C_{18}. The tier α fuel properties indicates that LJF is a good potential candidate to produce SAF-range compounds that are complementary to existing SAF pathways. Catalyst characterization methodologies suggested that Ru-HY-60-MI has small Ru size with good dispersion over HY-60 support. However, a catalyst deactivation was observed due to exchange of K^+ ion from lignin solution to HY-60 and carbon deposition on Ru-HY-60-MI surface during the experiment. Overall, this approach is a step forward towards continuous production of LJF based SAF with acceptable properties. However, we will continue advancing the process towards deployment by overcoming three main challenges: (1) decreasing the cost of the hydrotreating catalyst by replacing noble metal catalyst with base metals; (2) improving the relatively low efficiency of conventional solid catalysts due to the polymeric structure of lignin and, therefore the poor contact between the catalysts and lignin; and (3) hindering catalyst deactivations due to contaminants and coke formation. We wish that this work will be an effective and commercial relevant conversion technology to convert lignin into LJF with impactful volumes to achieve 100 % drop-in SAF goal.

CRediT authorship contribution statement

Adarsh Kumar: Writing – review & editing, Writing – original draft, Visualization, Methodology, Investigation, Formal analysis, Data curation, Conceptualization. **David C. Bell:** Writing – review & editing, Methodology, Formal analysis. **Zhibin Yang:** Writing – review & editing, Software, Methodology. **Joshua Heyne:** Writing – review & editing, Validation, Resources. **Daniel M. Santosa:** Validation, Formal analysis. **Huamin Wang:** Validation, Resources. **Peng Zuo:** Software, Methodology. **Chongmin Wang:** Software, Resources. **Ashutosh Mittal:** Writing – review & editing, Formal analysis. **Darryl P. Klein:** Resources, Formal analysis. **Michael J. Manto:** Formal analysis. **Xiaowen Chen:** Resources. **Bin Yang:** Writing – review & editing, Writing – original draft, Visualization, Validation, Supervision, Resources, Project administration, Methodology, Investigation, Funding acquisition, Formal analysis, Data curation, Conceptualization.

Declaration of competing interest

The authors declare that they have no known competing financial interests or personal relationships that could have appeared to influence the work reported in this paper.

Data availability

Data will be made available on request.

Acknowledgement

We are grateful for support from U.S. Department of Energy DOE-EERE Awards (DE-EE0009257) with the Bioproducts, Science & Engineering Laboratory and Department of Biological Systems Engineering at Washington State University. This work was done under the auspices of the WSU−PNNL Bioproducts Institute, which is a joint research collaboration of Washington State University and the U.S. Department of Energy's Pacific Northwest National Laboratory. A portion of the research was performed on a project award from the Environmental Molecular Sciences Laboratory, a DOE Office of Science User Facility sponsored by the Biological and Environmental Research program under Contract No. DE-AC05-76RL01830.

Appendix A. Supplementary data

Supplementary data to this article can be found online at https://doi.org/10.1016/j.fuproc.2024.108129.

References

[1] Department SR, Commercial Airlines Worldwide - Fuel Consumption 2005–2023, Available from: https://www.statista.com/statistics/655057/fuel-consumption-of-airlines-worldwide/#:~:text=The%20global%20fuel%20consumption%20by,95%20billion%20gallons%20in%202019, 2023.
[2] Group ATA, Waypoint 2050, Available from: https://aviationbenefits.org/media/167417/w2050_v2021_27sept_full.pdf, 2021.
[3] C. Voigt, J. Kleine, D. Sauer, R.H. Moore, T. Bräuer, P. Le Clercq, et al., Cleaner burning aviation fuels can reduce contrail cloudiness, Commun. Earth Environ. 2 (1) (2021) 114.
[4] K.S. Ng, D. Farooq, A. Yang, Global biorenewable development strategies for sustainable aviation fuel production, Renew. Sust. Energ. Rev. 150 (2021) 111502.
[5] J. Bai, Y. Zhang, X. Zhang, C. Wang, L. Ma, Synthesis of high-density components of jet fuel from lignin-derived aromatics via alkylation and subsequent hydrodeoxygenation, ACS Sustain. Chem. Eng. 9 (20) (2021) 7112–7119.
[6] B.S. Rana, R. Kumar, R. Tiwari, R. Kumar, R.K. Joshi, M.O. Garg, et al., Transportation fuels from co-processing of waste vegetable oil and gas oil mixtures, Biomass Bioenergy 56 (2013) 43–52.

[7] S. Karatzos, J.S. van Dyk, J.D. McMillan, J. Saddler, Drop-in biofuel production via conventional (lipid/fatty acid) and advanced (biomass) routes. Part I, Biofuels Bioprod. Biorefin. 11 (2) (2017) 344–362.

[8] Y. Lu, B. Ma, C. Zhao, Integrated production of bio-jet fuel containing lignin-derived arenes via lipid deoxygenation, Chem. Commun. 54 (70) (2018) 9829–9832.

[9] D. Verma, R. Kumar, B.S. Rana, A.K. Sinha, Aviation fuel production from lipids by a single-step route using hierarchical mesoporous zeolites, Energy Environ. Sci. 4 (5) (2011) 1667–1671.

[10] Z. Yang, Z. Xu, M. Feng, J.R. Cort, R. Gieleciak, J. Heyne, et al., Lignin-based jet fuel and its blending effect with conventional jet fuel, Fuel 321 (2022) 124040.

[11] S. Kosir, J. Heyne, J. Graham, A machine learning framework for drop-in volume swell characteristics of sustainable aviation fuel, Fuel 274 (2020) 117832.

[12] S. Kramer, G. Andac, J. Heyne, J. Ellsworth, P. Herzig, K.C. Lewis, Perspectives on fully synthesized sustainable aviation fuels: direction and opportunities, Front. Energy Res. 9 (2022) 1040.

[13] J.L. Graham, R.C. Striebich, K.J. Myers, D.K. Minus, W.E. Harrison, Swelling of nitrile rubber by selected aromatics blended in a synthetic jet fuel, Energy Fuel 20 (2) (2006) 759–765.

[14] survey Cwf, CRC report 647, Available from: https://crcao.org/crc-report-no-647/, 2006.

[15] M. Romanczyk, J.H. Ramirez Velasco, L. Xu, P. Vozka, P. Dissanayake, K.E. Wehde, et al., The capability of organic compounds to swell acrylonitrile butadiene O-rings and their effects on O-ring mechanical properties, Fuel 238 (2019) 483–492.

[16] S. Kosir, R. Stachler, J. Heyne, F. Hauck, High-performance jet fuel optimization and uncertainty analysis, Fuel 281 (2020) 118718.

[17] X. Luo, Q. Li, Effect of traditional solvent on thermal decomposition mechanism of lignin: a density functional theory study, Fuel Process. Technol. 258 (2024) 108093.

[18] H. Wang, Y. Pu, A. Ragauskas, B. Yang, From lignin to valuable products–strategies, challenges, and prospects, Bioresour. Technol. 271 (2019) 449–461.

[19] X. Yu, B. Yang, W. Zhu, T. Deng, Y. Pu, A. Ragauskas, et al., Towards functionalized lignin and its derivatives for high-value material applications, Ind. Crop. Prod. 200 (2023) 116824.

[20] P. Lei, J. Zhang, W. Shen, M. Zhong, S. Guo, Boosting the catalytic performance of Ru nanoparticles in the cleavage of β-O-4 linkages in lignin by doping Mo, Green Chem. 26 (11) (2024) 6616–6624.

[21] X. Zhang, Y. Jiang, W. Li, L. Zhu, L. Wang, Production of liquid fuels via catalytic transfer hydrogenation promoting lignin depolymerization on modified Y zeolite: Formic acid as a continuous hydrogen source, Energy Convers. Manag. 302 (2024) 118144.

[22] B. Yang, D.D. Laskar, Apparatus and process for preparing reactive lignin with high yield from plant biomass for production of fuels and chemicals. US Patent 9,518,076, 2016.

[23] B. Yang, H. Wang, Hydrodeoxygenation of lignin to hydrocarbons using bimetallic catalysts. US Patent US11078432B2, 2021.

[24] H. Wang, H. Ben, H. Ruan, L. Zhang, Y. Pu, M. Feng, et al., Effects of lignin structure on hydrodeoxygenation reactivity of pine wood lignin to valuable chemicals, ACS Sustain. Chem. Eng. 5 (2) (2017) 1824–1830.

[25] H. Wang, Y. Duan, Q. Zhang, B. Yang, Effects of sugars, furans, and their derivatives on hydrodeoxygenation of biorefinery lignin-rich wastes to hydrocarbons, ChemSusChem 11 (15) (2018) 2562–2568.

[26] H. Wang, M. Feng, B. Yang, Catalytic hydrodeoxygenation of anisole: an insight into the role of metals in transalkylation reactions in bio-oil upgrading, Green Chem. 19 (7) (2017) 1668–1673.

[27] H. Wang, H. Ruan, M. Feng, Y. Qin, H. Job, L. Luo, et al., One-pot process for hydrodeoxygenation of lignin to alkanes using Ru-based bimetallic and bifunctional catalysts supported on zeolite Y, ChemSusChem 10 (8) (2017) 1846–1856.

[28] H. Wang, H. Ruan, H. Pei, H. Wang, X. Chen, M.P. Tucker, et al., Biomass-derived lignin to jet fuel range hydrocarbons via aqueous phase hydrodeoxygenation, Green Chem. 17 (12) (2015) 5131–5135.

[29] H. Wang, H. Wang, E. Kuhn, M.P. Tucker, B. Yang, Production of jet fuel-range hydrocarbons from hydrodeoxygenation of lignin over super Lewis acid combined with metal catalysts, ChemSusChem 11 (1) (2017) 285–291.

[30] H. Wang, B. Yang, Q. Zhang, W. Zhu, Catalytic routes for the conversion of lignocellulosic biomass to aviation fuel range hydrocarbons, Renew. Sust. Energ. Rev. 120 (2020) 109612.

[31] H. Wang, L. Zhang, T. Deng, H. Ruan, X. Hou, J.R. Cort, et al., ZnCl 2 induced catalytic conversion of softwood lignin to aromatics and hydrocarbons, Green Chem. 18 (9) (2016) 2802–2810.

[32] H. Ruan, Y. Qin, J. Heyne, R. Gieleciak, M. Feng, B. Yang, Chemical compositions and properties of lignin-based jet fuel range hydrocarbons, Fuel 256 (2019) 115947.

[33] D.D. Laskar, M.P. Tucker, X. Chen, G.L. Helms, B. Yang, Noble-metal catalyzed hydrodeoxygenation of biomass-derived lignin to aromatic hydrocarbons, Green Chem. 16 (2) (2014) 897–910.

[34] D.D. Laskar, B. Yang, H.M. Wang, J. Lee, Pathways for biomass-derived lignin to hydrocarbon fuels, Biofuels Bioproducts Biorefining-Biofpr 7 (5) (2013) 602–626.

[35] H. Wang, M. Feng, B. Yang, Catalytic hydrodeoxygenation of anisole: an insight into the role of metals in transalkylation reactions in bio-oil upgrading, Green Chem. 19 (2017) 1668–1673.

[36] L. Zhang, T.L. Butler, Bin Yang*, Recent trends, opportunities and challenges of sustainable aviation fuel, Green Energy Sustain. (2020) 85–110.

[37] H. Wang, B. Yang, Q. Zhang, W. Zhu, Catalytic routes for the conversion of lignocellulosic biomass to aviation fuel range hydrocarbons, Renew. Sust. Energ. Rev. 120 (2020) 109612.

[38] M.L. Stone, M.S. Webber, W.P. Mounfield, D.C. Bell, E. Christensen, A.R.C. Morais, et al., Continuous hydrodeoxygenation of lignin to jet-range aromatic hydrocarbons, Joule 6 (10) (2022) 2324–2337.

[39] J. Löfstedt, C. Dahlstrand, A. Orebom, G. Meuzelaar, S. Sawadjoon, M.V. Galkin, et al., Green diesel from kraft lignin in three steps, ChemSusChem 9 (12) (2016) 1392–1396.

[40] D. Di Francesco, C. Dahlstrand, J. Löfstedt, A. Orebom, J. Verendel, C. Carrick, et al., Debottlenecking a pulp mill by producing biofuels from black liquor in three steps, ChemSusChem 14 (11) (2021) 2414–2425.

[41] K. Johnson, T. Loegel, A. Metz, P. Wrzesinski, L. Shafer, R. Striebich, et al., Method for Detailed Hydrocarbon Analysis of Middle Distillate Fuels by Two-Dimensional Gas Chromatography, 2020.

[42] S.R. Bare, F.D. Vila, M.E. Charochak, S. Prabhakar, W.J. Bradley, C. Jaye, et al., Characterization of coke on a Pt-Re/γ-Al2O3 Re-forming catalyst: experimental and theoretical study, ACS Catal. 7 (2) (2017) 1452–1461.

[43] D.D. Laskar, M.P. Tucker, X. Chen, G.L. Helms, B. Yang, Noble-metal catalyzed hydrodeoxygenation of biomass-derived lignin to aromatic hydrocarbons, Green Chem. 16 (2014).

[44] Y. He, X. Li, H. Ben, X. Xue, B. Yang, Lipid production from dilute alkali corn Stover lignin by Rhodococcus strains, ACS Sustain. Chem. Eng. 5 (3) (2017) 2302–2311.

[45] H. Ruan, Z. Xu, A. Kumar, M. Feng, A.S. Lipton, E.D. Walter, et al., Elucidating the reaction pathways of veratrylglycero-β-guaiacyl ether degradation over metal-free solid acid catalyst with hydrogen, ChemSusChem 16 (6) (2023) e202202001.

[46] R. Singh, A. Prakash, S.K. Dhiman, B. Balagurumurthy, A.K. Arora, S.K. Puri, et al., Hydrothermal conversion of lignin to substituted phenols and aromatic ethers, Bioresour. Technol. 165 (2014) 319–322.

[47] J. Marlowe, P.C. Ford, M.M. Abu-Omar, P. Christopher, Structure sensitivity in Pt-catalyzed hydrodeoxygenation of multi-oxygenated lignol model compounds, Cat. Sci. Technol. 13 (19) (2023) 5662–5678.

[48] W. Liu, W. You, W. Sun, W. Yang, A. Korde, Y. Gong, et al., Ambient-pressure and low-temperature upgrading of lignin bio-oil to hydrocarbons using a hydrogen buffer catalytic system, Nat. Energy 5 (10) (2020) 759–767.

[49] X. Jin, R. Tsukimura, T. Aihara, H. Miura, T. Shishido, K. Nozaki, Metal–support cooperation in Al(PO3)3-supported platinum nanoparticles for the selective hydrogenolysis of phenols to arenes, Nat. Catal. 4 (4) (2021) 312–321.

[50] Z. Xiang, W. Wang, F. Zhou, H. Zhang, Y. Wang, W. Zhu, et al., Efficient conversion of lignin-derived phenols to cycloalkanes over bifunctional catalysts with low loading of ruthenium, Fuel Process. Technol. 256 (2024) 108073.

[51] H. Wang, H. Wang, E. Kuhn, M.P. Tucker, B. Yang, Production of jet fuel-range hydrocarbons from hydrodeoxygenation of lignin over super Lewis acid combined with metal catalysts, ChemSusChem 11 (1) (2018) 285–291.

[52] H. Wang, H. Ruan, M. Feng, Y. Qin, H. Job, L. Luo, et al., One-pot process for hydrodeoxygenation of lignin to alkanes using Ru-based bimetallic and bifunctional catalysts supported on zeolite Y, ChemSusChem 10 (8) (2017) 1846–1856.

[53] A. Kumar, A. Kumar, D.M. Santosa, H. Wang, P. Zuo, C. Wang, et al., Engineered Ru on HY zeolite catalyst for continuous and selective hydrodeoxygenation of lignin phenolics to cycloalkanes under moderate conditions, Appl. Catal. A Gen. 676 (2024) 119649.

[54] L. Nie, B. Peng, X. Zhu, Vapor-phase hydrodeoxygenation of guaiacol to aromatics over Pt/HBeta: Identification of the role of acid sites and metal sites on the reaction pathway, ChemCatChem 10 (5) (2018) 1064–1074.

[55] A. Selvarajoo, D. Oochit, Effect of pyrolysis temperature on product yields of palm fibre and its biochar characteristics, Mater. Sci. Energy Technol. 3 (2020) 575–583.

[56] V. Dhyani, T. Bhaskar, A comprehensive review on the pyrolysis of lignocellulosic biomass, Renew. Energy 129 (2018) 695–716.

[57] M. Žula, M. Grilc, B. Likozar, Hydrocracking, hydrogenation and hydro-deoxygenation of fatty acids, esters and glycerides: Mechanisms, kinetics and transport phenomena, Chem. Eng. J. 444 (2022) 136564.

[58] Z. Cao, Y. Xu, P. Lyu, M. Dierks, Á. Morales-García, W. Schrader, et al., Flexibilization of biorefineries: tuning lignin hydrogenation by hydrogen partial pressure, ChemSusChem 14 (1) (2021) 373–378.

[59] H. Duan, J. Dong, X. Gu, Y.-K. Peng, W. Chen, T. Issariyakul, et al., Hydrodeoxygenation of water-insoluble bio-oil to alkanes using a highly dispersed Pd–Mo catalyst, Nat. Commun. 8 (1) (2017) 591.

[60] P. Yan, G. Bryant, M.M.-J. Li, J. Mensah, E. Kennedy, M. Stockenhuber, Shape selectivity of zeolite catalysts for the hydrodeoxygenation of biocrude oil and its model compounds, Microporous Mesoporous Mater. 309 (2020) 110561.

[61] A.V. Vutolkina, I.G. Baigildin, A.P. Glotov, A.A. Pimerzin, A.V. Akopyan, A. L. Maximov, et al., Hydrodeoxygenation of guaiacol via in situ H2 generated through a water gas shift reaction over dispersed NiMoS catalysts from oil-soluble precursors: Tuning the selectivity towards cyclohexene, Appl. Catal. B Environ. 312 (2022) 121403.

[62] A. Gutiérrez, J.M. Arandes, P. Castaño, M. Olazar, A. Barona, J. Bilbao, Effect of space velocity on the hydrocracking of Light Cycle Oil over a Pt–Pd/HY zeolite catalyst, Fuel Process. Technol. 95 (2012) 8–15.

[63] Y. Jing, M. Shakouri, X. Liu, Y. Hu, Y. Guo, Y. Wang, Breaking C—C bonds and preserving C—O bonds in aromatic plastics and lignin via a reversing bond energy cleavage strategy, ACS Catal. 12 (17) (2022) 10690–10699.

[64] X. Wu, X. Fan, S. Xie, J. Lin, J. Cheng, Q. Zhang, et al., Solar energy-driven lignin-first approach to full utilization of lignocellulosic biomass under mild conditions, Nat. Catal. 1 (10) (2018) 772–780.

[65] Y. Li, L. Shuai, H. Kim, A.H. Motagamwala, J.K. Mobley, F. Yue, et al., An "ideal lignin" facilitates full biomass utilization, Sci. Adv. 4 (9) (2018) eaau2968.
[66] M. Khosravi, V. Murthy, D.R. Mackinnon, I., The exchange mechanism of alkaline and alkaline-earth ions in zeolite N, Molecules 24 (20) (2019) 3652.
[67] Z. Yang, S. Kosir, R. Stachler, L. Shafer, C. Anderson, J.S. Heyne, A GC × GC Tier α combustor operability prescreening method for sustainable aviation fuel candidates, Fuel 292 (2021) 120345.
[68] J. Heyne, D. Bell, J. Feldhausen, Z. Yang, R. Boehm, Towards fuel composition and properties from Two-dimensional gas chromatography with flame ionization and vacuum ultraviolet spectroscopy, Fuel 312 (2022) 122709.
[69] D. Luning Prak, J. Cooke, T. Dickerson, A. McDaniel, J. Cowart, Cetane number, derived cetane number, and cetane index: when correlations fail to predict combustibility, Fuel 289 (2021) 119963.
[70] R. Lanza, S.G. Järås, P. Canu, Partial oxidation of methane over supported ruthenium catalysts, Appl. Catal. A Gen. 325 (1) (2007) 57–67.
[71] D.C. Elliott, H. Wang, R. French, S. Deutch, K. Iisa, Hydrocarbon liquid production from biomass via hot-vapor-filtered fast pyrolysis and catalytic hydroprocessing of the bio-oil, Energy Fuel 28 (9) (2014) 5909–5917.
[72] A. Kumar, A. Kumar, B. Biswas, J. Kumar, S.R. Yenumala, T. Bhaskar, Hydrodeoxygenation of m-Cresol over Ru based catalysts: Influence of catalyst support on m-Cresol conversion and methylcyclohexane selectivity, Renew. Energy 151 (2020) 687–697.
[73] Q. Yao, Z.-H. Lu, K. Yang, X. Chen, M. Zhu, Ruthenium nanoparticles confined in SBA-15 as highly efficient catalyst for hydrolytic dehydrogenation of ammonia borane and hydrazine borane, Sci. Rep. 5 (1) (2015) 15186.
[74] S. Shwan, J. Jansson, L. Olsson, M. Skoglundh, Effect of post-synthesis hydrogen-treatment on the nature of iron species in Fe-BEA as NH 3-SCR catalyst, Cat. Sci. Technol. 4 (9) (2014) 2932–2937.
[75] X. Wu, Z. Wang, D. Zhang, Y. Qin, M. Wang, Y. Han, et al., Solvent-free microwave synthesis of ultra-small Ru-Mo2C@ CNT with strong metal-support interaction for industrial hydrogen evolution, Nat. Commun. 12 (1) (2021) 4018.
[76] G. Xiang, X. Shi, Y. Wu, J. Zhuang, X. Wang, Size effects in atomic-level epitaxial redistribution process of RuO2 over TiO2, Sci. Rep. 2 (1) (2012) 801.
[77] C. Liu, G. Li, E.J.M. Hensen, E.A. Pidko, Relationship between acidity and catalytic reactivity of faujasite zeolite: a periodic DFT study, J. Catal. 344 (2016) 570–577.
[78] J. Hou, J. Yuan, R. Shang, Synthesis and characterization of zeolite W and its ion-exchange properties to K+ in seawater, Powder Technol. 226 (2012) 222–224.
[79] E. Heracleous, E. Pachatouridou, A.M. Hernández-Giménez, H. Hernando, T. Fakin, A.L. Paioni, et al., Characterization of deactivated and regenerated zeolite ZSM-5-based catalyst extrudates used in catalytic pyrolysis of biomass, J. Catal. 380 (2019) 108–122.